J|A|C|S
ARTICLES
Published on Web 04/05/2006

Detailed Structure of Diamond-Type Lipid Cubic Nanoparticles

Borislav Angelov,[†] Angelina Angelova,*[,‡] Brigitte Papahadjopoulos-Sternberg,[§] Sylviane Lesieur,[‡] Jean-François Sadoc,[⊥] Michel Ollivon,[‡] and Patrick Couvreur[‡]

Contribution from the Institute of Biophysics, Bulgarian Academy of Sciences, Acad. G. Bonchev Str. Bl.21, BG-1113 Sofia, Bulgaria, Physico-chimie, Pharmacotechnie, Biopharmacie, UMR8612 CNRS, University of Paris XI, 5 Rue J.B. Clément, F-92290 Châtenay-Malabry, France, NanoAnalytical Laboratory, San Francisco, California 94118, and Laboratoire de Physique des Solides, UMR8502 CNRS, Université de Paris Sud, Bât. 510, F-91405 Orsay, France

Received January 5, 2006; E-mail: angelina.angelova@cep.u-psud.fr

Abstract: Supramolecular three-dimensional self-assembly of nonlamellar lipids with fragments of the protein immunoglobulin results in a bicontinuous cubic phase fragmented into nanoparticles with open water channels (cubosomes). The structure of the diamond-type cubic nanoparticles is characterized experimentally by freeze−fracture electron microscopy, and it is mathematically modeled with nodal surfaces emphasizing the fluid-like undulations of the cubosomic interfaces. Based on scaling-up and scaling-down approaches, we present stable and intermediate-kind nanoparticles resulting from the cubosomic growth. Our results reveal the smallest stable diamond-type cubosomic entity that can serve as a building block of more complex nanostructured fluid drug delivery vehicles of therapeutic proteins. The evidence presented for lipid-bilayer undulations in the surface region of the protein/lipid cubosomes could have important consequences for possible applications of these hierarchically organized porous nanoparticles.

Introduction

Controlling fluid-phase nanopatterning via hierarchical self-assembly and pattern formation in nanostructured fluids are currently problems of fundamental significance for innovations in soft-matter nanotechnology.[1−4] Owing to their versatile structural organization, nanostructured complex fluid networks and dispersions of amphiphiles enable soft-matter applications in advanced pharmaceutical formulations and delivery systems, membrane-based materials, biocatalysis, self-assembly gels, and personal care and food nanotechnology products.[4−14] Fascinating patterns of complex cubic topologies occur in biological systems (three-dimensional (3D) cubic membranes in echinoids, stratum corneum, mitochondria, and prolamellar body) as well as in self-assembly supramolecular systems with enhanced surface-to-volume ratio.[15−27] Bicontinuous cubic phases (BCPs) formed

[†] Bulgarian Academy of Sciences.
[‡] University of Paris XI.
[§] NanoAnalytical Laboratory.
[⊥] Université de Paris Sud.

(1) (a) Nekovee, M.; Coveney, P. V. *J. Am. Chem. Soc*. **2001**, *123*, 12380−12382. (b) Marrink, S.-J.; Tieleman, D. P. *J. Am. Chem. Soc*. **2001**, *123*, 12383−12391.
(2) Hyde, S.; Andersson, S.; Larsson, K.; Blum, Z.; Landh, T.; Lidin, S.; Ninham, B. W. *The Language of Shape*; Elsevier Science: New York, 1996.
(3) (a) Kline, T. R.; Paxton, W. F.; Wang, Y.; Velegol, D.; Mallouk, T. E.; Sen, A. *J. Am. Chem. Soc.* **2005**, *127*, 17150−17151. (b) Hernandez, R. M.; Richter, L.; Semancik, S.; Stranick, S.; Mallouk, T. E. *Chem. Mater.* **2004**, *16*, 3431−3438.
(4) Knoll, A.; Lyakhova, K. S.; Horvat, A.; Krausch, G.; Sevink, G. J. A.; Zvelindovsky, A. V.; Magerle, R. *Nat. Mater*. **2004**, *3*, 886−890.
(5) (a) Holyst, R. *Nat. Mater*. **2005**, *4*, 510−511. (b) Garstecki, P.; Holyst, R. *Langmuir* **2002**, *18*, 2529−2537.
(6) (a) Allen, T.; Cullis, P. R. *Science* **2004**, *303*, 1818−1822. (b) Martina, M.-S.; Fortin, J.-P.; Menager, C.; Clement, O.; Barratt, G.; Grabielle-Madelmont, C.; Gazeau, F.; Cabuil, V.; Lesieur, S. *J. Am. Chem. Soc.* **2005**, *127*, 10676−10685. (c) Lesieur, S.; Grabielle-Madelmont, C.; Menager, C.; Cabuil, V.; Dadhi, D.; Pierrot, P.; Edwards, K. *J. Am. Chem. Soc.* **2003**, *125*, 5266−5267.
(7) Sternberg, B.; Moody, M. F.; Yoshioka, T.; Florence, A. T. *Nature* **1995**, *378*, 21.
(8) Kisak, E. T.; Coldren, B.; Evans, C. A.; Boyer, C.; Zasadzinski, J. A. *Curr. Med. Chem.* **2004**, *11*, 199−219.
(9) Discher, B. M.; Won, Y.-Y.; Ege, D. S.; Lee, J. C−M.; Bates, F. S.; Discher, D. E.; Hammer, D. A. *Science* **1999**, *284*, 1143−1146.
(10) Douglas, T.; Young, M. *Nature* **1998**, *393*, 152−155.
(11) Ravindra, R.; Zhao, S.; Gies, H.; Winter, R. *J. Am. Chem. Soc.* **2004**, *126*, 12224−12225.
(12) Zeng, X.; Ungar, G.; Impéror-Clerc, M. *Nat. Mater*. **2005**, *4*, 562−567.
(13) (a) Spicer, P. T.; Small, W. E.; Lynch, M. L.; Burns, J. L. *J. Nanopart. Res.* **2002**, *4*, 297−311. (b) Spicer, P. T. *Curr. Opin. Colloid Interface Sci.* **2005**, *10*, 274−279.
(14) Mezzenga, R.; Schurtenberger, P.; Burbidge, A.; Michel, M. *Nat. Mater*. **2005**, *4*, 729−740.
(15) Landh, T. *FEBS Lett*. **1995**, *369*, 13−17.
(16) Nissen, H.-U. *Science* **1969**, *166*, 1150−1152.
(17) Norlén, L.; Al-Amoudi, A. *J. Invest. Dermatol*. **2004**, *123*, 715−732.
(18) Deng, Y. R.; Marko, M.; Buttle, K. F.; Leith, A.; Mieczkowski, M.; Mannella, CA. *J. Struct. Biol.* **1999**, *127*, 231−239.
(19) (a) Zhao, D.; Feng, J.; Huo, O.; Melosh, N.; Fredrickson, G. H.; Chmelka, B. F.; Stucky, G. D. *Science* **1998**, *279*, 548−552. (b) Alfredsson, V.; Anderson, M. W.; Ohsuna, T.; Terasaki, O.; Jacob, M.; Bojrup, M. *Chem. Mater.* **1997**, *9*, 2066−2070.
(20) Buchheim, W.; Larsson, K. *J. Colloid Interface Sci*. **1987**, *117*, 582−583.
(21) (a) Gustafsson, J.; Ljusberg-Wahren, H.; Almgren, M.; Larsson, K. *Langmuir* **1996**, *12*, 4611−4613. (b) Nakano, M.; Sugita, A.; Matsuoka, H.; Handa, T. *Langmuir* **2001**, *17*, 3917−3922.
(22) Almgren, M.; Edwards, K.; Karlsson, G. *Colloids Surf. A* **2000**, *174*, 3−21.
(23) Barauskas, J.; Johnsson, M.; Joabsson, F.; Tiberg, F. *Langmuir* **2005**, *21*, 2569−2577.
(24) (a) Benedicto, A. D.; O'Brien, D. F. *Macromolecules* **1997**, *30*, 3395−3402. (b) Anderson, D. M.; Davis, H. T.; Scriven, L. E.; Nitsche, J. C. C. *Adv. Chem. Phys.* **1990**, *77*, 337−396.
(25) Borné, J.; Nylander, T.; Khan, A. *J. Phys. Chem. B* **2002**, *106*, 10492−10500.
(26) Angelova, A.; Angelov, B.; Papahadjopoulos-Sternberg, B.; Ollivon, M.; Bourgaux, C. *Langmuir* **2005**, *21*, 4138−4143.
(27) Angelova, A.; Angelov, B.; Papahadjopoulos-Sternberg, B.; Bourgaux, C.; Couvreur, P. *J. Phys. Chem. B* **2005**, *109*, 3089−3093.

by amphiphiles in water are complex fluid systems with a high degree of symmetry and a periodic nanochannel organization.[2,5,28−33] They permit nanoencapsulation of drugs[34,35] and synthesis in confined space.[36] BCPs can serve as carriers of various proteins[28,37−46] (including water-soluble recombinant proteins of therapeutic interest)[26,45] as well as templates to guide or orient the growth of nanostructures, biomolecular scaffolds, or protein crystals.[13,25,42,47−50] The labyrinthine water-channel networks in biocompatible amphiphilic cubic assemblies have been characterized by aqueous channel diameters between 3 and 7 nm at full hydration.[37,50]

Finite nanoparticles of BCPs, recognized as cubosomes,[51] should interact with the biological environment and with sites for targeting through their complex interfaces involving the inherent open nanofluidic channels. The role of the cubosomic surface essentially increases in nanotechnology applications, where the fragmentation and dispersion of a bulk amphiphilic liquid-crystalline phase into nanoparticles[21−23] generates a huge 3D fluid interface of a hierarchical organization.[13,26] The porous interface architecture with a controllable channel size presents advantages for controlled release and uptake applications, as the number of nanochannels available to interact with biological media in cubic mesostructures is essentially greater than that in other nanocompartment systems (hexosomes, spongosomes, vesicles, polymersomes, vesosomes, nanotubules, etc). Spicer[13b] has recently reviewed the advances in and the prospective applications of cubosomes.

While the entrapment of biomolecules in host supramolecular cubic lipid systems at low hydration levels has received considerable attention,[20,28,35,39−44,47−49] the mechanism of nucleation and growth of a stable cubosome at high hydration as well as the destiny of the smallest stable cubosomic entity upon the encapsulation of protein macromolecules has not been addressed in a bottom-up investigation. The formation of proteocubosome carriers, stable at high hydration levels in excess aqueous phase, has recently been reported,[26] and the functionalization of lipid cubic phases by synthetic lipids has been proposed in relation to biomedical applications.[37]

Experimental data[26] have indicated that proteocubosomic nano-objects could be created by fragmentation of a bulk cubic (lipid/protein/water) phase, which generates cubosomes.[13,21−23] Here we investigate in detail the diamond-type (D-type) cubic supramolecular structure of functionalized cubosomic assemblies. They were created by full hydration of the amphiphile monoolein (MO) mixed with a synthetic lipid with a triethyleneglycol spacer in the reactive polar headgroup (MTEG), following by encapsulation of protein (Fab fragments of immunoglobulin). The cubic liquid-crystalline organization of the fully hydrated systems was determined by means of synchrotron X-ray diffraction. By means of freeze−fracture electron microscopy we analyzed the supramolecular structure modifications induced by the guest biomolecules (MTEG lipid and Fab protein) incorporated into the host cubic lattice. This approach permitted us to identify the architectures revealing the protein-directed patterning of the cubosomic topologies and their scaling-down to nanosized entities. The aim was to characterize the smallest cubosomic structural unit (nanocubosome) built-up from D-type cubosomic nanochannels. We investigated theoretically the mechanism by which a diamond-type cubosomic nano-object takes shape.

Methods

Supramolecular Structure Modelization. Cubosomic surfaces were modeled here as nodal surfaces using the recently introduced method of so-called "handmade" structures.[52,53] In our own implementation of this method, we generated a diamond-type structure that consists of 7 × 7 × 7 unit cells. From this large box, only the nodes that are within a sphere of a given radius were selected. The center of the sphere coincided with the center of the 7 × 7 × 7 box. The second step was to construct the Gaussian distribution function for every node *N*. We used the following expression for the Gaussian distribution:

$$\exp\left(-\frac{(x-x_i)^2+(y-y_i)^2+(z-z_i)^2}{2s^2}\right)/(\sqrt{2\pi}s)$$

where x_i, y_i, and z_i are the coordinates of the nodes and s is the standard deviation. The value of s is equal for all nodes. It was chosen to fit the sine function using Gaussian distributions. In our case, when the 7 × 7 × 7 box was scaled in the range from −1 to 1 in the x, y, and z directions, the value of $s = 0.0495$ was obtained. In a third step, we chose the surface that is closest to the minimal surface when the "handmade" structure is periodic. For all presented nodal surfaces, the

(28) Mariani, P.; Luzzati, V.; Delacroix, H. *J. Mol. Biol.* **1988**, *204*, 165−188.
(29) (a) Luzzati, V. *Curr. Opin. Struct. Biol.* **1997**, *7*, 661−668. (b) Luzzati, V.; Vargas, R.; Mariani, P.; Gulik, A.; Delacroix, H. *J. Mol. Biol.* **1993**, *229*, 540−551.
(30) Luzzati, V.; Delacroix, H.; Gulik, A.; GulikKrzywicki, T.; Mariani, P.; Vargas, R. *Lipid Polymorphism Membr. Prop.* **1997**, *44*, 3−24.
(31) (a) Gruner, S. M. *J. Phys. Chem.* **1989**, *93*, 7562−7570. (b) Schwarz, U. S.; Gompper, G. *Phys. Rev. E* **1999**, *59*, 5528−5541
(32) Lindblom, G.; Larsson, K.; Johansson, L.; Fontell, K.; Forsen, S. *J. Am. Chem. Soc.* **1979**, *101*, 5465−5470.
(33) (a) Squires, A. M.; Templer, R. H.; Seddon, J. M.; Woenckhaus, J.; Winter, R.; Finet, S.; Theyencheri, N. *Langmuir* **2002**, *18*, 7384−7392. (b) Vacklin, H.; Khoo, B. J.; Madan, K. H.; Seddon, J. M.; Templer, R. H. *Langmuir* **2000**, *16*, 4741−4748. (c) Funari, S. S.; Rapp, G. *Proc. Natl. Acad. Sci. U.S.A.* **1999**, *96*, 7756−7759.
(34) (a) Ericsson, B.; Eriksson, P. O.; Löfroth, J. E.; Engström, S. *ACS Symp. Ser. (Polym. Drugs, Drug Delivery Syst.)* **1991**, *469*, 251−265. (b) Carlsson, N.; Winge, A.-S.; Engstrom, S.; Akerman, B. *J. Phys. Chem. B* **2005**, *109*, 18628−18636.
(35) (a) Caboi, F.; Nylander, T.; Razumas, V.; Talaikyte, Z.; Monduzzi, M.; Larsson, K. *Langmuir* **1997**, *13*, 5476−5483. (b) Persson, G.; Edlund, H.; Lindblom, G. *Eur. J. Biochem.* **2003**, *270*, 56−65.
(36) Puvvada, S.; Baral, S.; Chow, G. M.; Qadri, S. B.; Ratna, B. R. *J. Am. Chem. Soc.* **1994**, *116*, 2135−2136.
(37) Angelova, A.; Ollivon, M.; Campitelli, A.; Bourgaux, C. *Langmuir* **2003**, *19*, 6928−6935.
(38) Angelova, A.; Angelov, B.; Papahadjopoulos-Sternberg, B.; Ollivon, M.; Bourgaux, C. *J. Drug Delivery Sci. Technol.* **2005**, *15*, 108−112.
(39) Kraineva, J.; Narayanan, R. A.; Kondrashkina, E.; Thiyagarajan, P.; Winter, R. *Langmuir* **2005**, *21*, 3559−3571.
(40) Landau, E. M.; Luisi, P. L. *J. Am. Chem. Soc.* **1993**, *115*, 2102−2106.
(41) Portmann, M.; Landau, E. M.; Luisi, P. L. *J. Phys. Chem.* **1991**, *95*, 8437−8440.
(42) Leslie, S. B.; Puvvada, S.; Ratna, B. R.; Rudolph, A. S. *Biochim. Biophys. Acta* **1996**, *1285*, 246−254.
(43) Razumas, V.; Larsson, K.; Miezis, Y.; Nylander, T. *J. Phys. Chem.* **1996**, *100*, 11766−11774.
(44) Ericsson, B.; Larsson, K.; Fontell, K. *Biochim. Biophys. Acta* **1983**, *729*, 23−27.
(45) Shah, J. C.; Sadhale, Y.; Chilukuri, D. M. *Adv. Drug Delivery Rev.* **2001**, *47*, 229−250
(46) (a) Clogston, J.; Caffrey, M. *J. Controlled Release* **2005**, *107*, 97−111. (b) Liu, M.; Caffrey, M. *J. Struct. Biol.* **2005**, *150*, 23−40. (c) Giorgione, J. R.; Huang, Z.; Epand, R. M. *Biochemistry* **1998**, *37*, 2384−2392.
(47) Nollert, P.; Navarro, J.; Landau, E. M. *Methods Enzymol.* **2002**, *343*, 183−199.
(48) (a) Nollert, P. *Prog. Biophys. Mol. Biol.* **2005**, *88*, 339−357. (b) Caffrey, M. *J. Struct. Biol.* **2003**, *142*, 108−132.
(49) (a) Landau, E. M.; Rosenbusch, J. P. *Proc. Natl. Acad. Sci. U.S.A.* **1996**, *93*, 14532−14535. (b) Pebay-Peyroula, E.; Rummel, G.; Rosenbusch, J. P.; Landau, E. M. *Science* **1997**, *277*, 1676−1681.
(50) Angelov, B.; Angelova, A.; Ollivon, M.; Bourgaux, C.; Campitelli, A. *J. Am. Chem. Soc.* **2003**, *125*, 7118−7189.
(51) Larsson, K. *J. Phys. Chem.* **1989**, *93*, 3, 7304−7314.
(52) Jacob, M.; Andersson, S. *The nature of mathematics and the mathematics of nature*; Elsevier: Amsterdam, 1998; pp 191−225.
(53) Andersson, S.; Larsson, K.; Larsson, M.; Jacob, M. *Biomathematics: Mathematics of biostructures and biodynamics*; Elsevier: Amsterdam, 1999: pp 131−162.

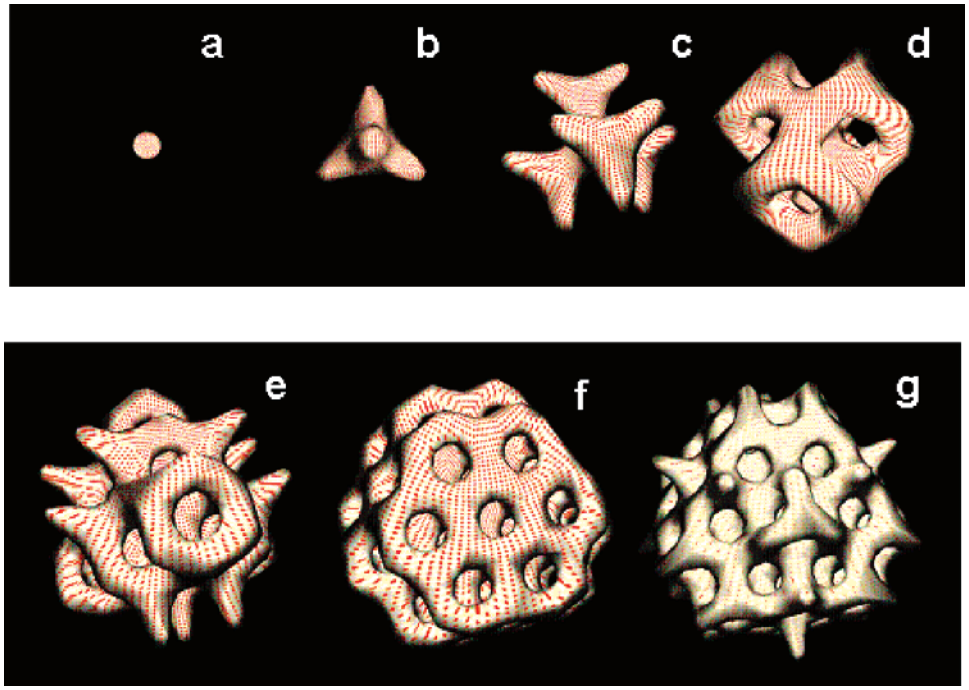

Figure 1. "Bottom-up" mechanism of the 3D growth of a cubosomic nano-object represented by nodal surfaces that form diamond-type skeletons of nanochannels. Note that the cubosome, generated from a curved lipid bilayer, adopts only discrete sizes upon growth. The latter is determined by geometrical constraints for preservation of the lipid bilayer integrity in the cubic lattice skeleton. The presented stages of cubosomal nanostructure growth correspond to (a) $N = 1$; (b) $N = 5$; (c) $N = 17$; (d) $N = 29$; (e) $N = 71$; (f) $N = 147$; and (g) $N = 191$ (where N is the number of nodes (repeat volumes) in the nano-object).

total sum of the Gaussian distribution functions was set to be equal to $c_m = 7.8255$ (c_m is the constant by which we selected the nodal surface that is closest to the minimal one). This yielded periodic nodal surfaces inside the diamond-type cubosomes.

Sample Preparation. We used monoolein (MO; Sigma, purity >99.5%) as a main nonlamellar lipid component, and 1-{8-[4-(*p*-maleimidophenyl)butaroylamino]-3,6-dioxaloctyl}-2,3-distearyl glyceryl DL-ether (MTEG; Northern Lipids Inc., purity >99.5%) served as a guest ether lipid with a triethylene glycol moiety in the polar group. Aqueous phase was prepared with 0.1 M NaCl and 10^{-2} M phosphate buffer (pH 7). The lipids MO and MTEG were mixed in chloroform at a molar ratio 98/2, and the solvent was evaporated under nitrogen gas flow during at least 4 h. The lyophilized dry lipid mixture was hydrated in excess aqueous buffer phase of Fab fragments of human chrompure immunoglobulin (Jackson ImmunoResearch Laboratories Inc.). A self-assembly lipid/protein system was generated via repeated vortexing and incubation cycles (20 min each) at 37 °C. The samples were equilibrated and stored at 4 °C.

Freeze−Fracture Electron Microscopy. For freeze−fracture electron microscopy (FF-EM), the samples were quenched using the sandwich technique and liquid-nitrogen-cooled propane. Using this technique, a cooling rate of 10 000 K s^{-1} is reached, avoiding ice crystal formation and artifacts possibly caused by the cryo-fixation process. The cryo-fixed samples were stored in liquid nitrogen for less than 2 h before processing. The fracturing process was carried out in JEOL JED-9000 freeze-etching equipment, and the exposed fracture planes were shadowed with Pt for 30 s at an angle of 25−35° and with C for 35 s (2 kV/60−70 mA, 1×10^{-5} Torr). The replicas produced this way were cleaned with concentrated, fuming HNO_3 for 24 h, followed by repeated agitation with fresh chloroform/methanol (1:1 v/v) at least five times. The replicas cleaned this way were examined using a JEOL 100 CX electron microscope.

Image Analysis. 3D reconstructions from raw FF-EM images were realized by using the software SPIP (The Scanning Probe Image Processor) from Image Metrology. The module 3D Visualization Studio was used in the image processing.

Results and Discussion

Here, using nodal surfaces, we reconstruct a "bottom-up" mechanism of growth of a diamond-type cubic network of aqueous channels starting from a curved lipid bilayer nucleus (nanovesicle). The diameter of the curved lipid bilayer unit (Figure 1a) corresponds to the sum of the thickness of two lipid bilayers and the diameter of one aqueous nanochannel. The presented nanovesicle has a diameter of 8.8 nm. We generated diverse cubosomic nanostructures as a function of the number, N, of repeated elementary unit volumes (nodes) in the growing nanochannel network (see the section, Supramolecular Structure Modelization).

The 3D cubosomic structures modeled in Figure 1b−g represent selected stages in the growth of the nanochannel architecture, starting from a single nanovesicle and building-up a cubosomic assembly from up to hundreds of nodes. Figure 1 reveals that some of the growing scaffolds (e.g., those at $N = 71$ and at $N = 191$) involve protrusions, resulting in unstable lipid membrane configurations. For a pattern of aqueous nanochannels to be stable upon cubosomal growth, the generated cubosomic surfaces should not be terminated by closed water channels. This requirement is satisfied, for instance, with $N = 29$ and $N = 147$, where $N = 29$ yields the first stable lipid bilayer configuration described internally by a diamond-type periodic surface.

We explore the advantages of high-resolution FF-EM[7,54,55] for direct visualization of the internal structure of 3D cubosomic

(54) (a) Sternberg, B.; Hong, K.; Zheng, W.; Papahadjopoulos, D. *Biochim. Biophys. Acta* **1998**, *1375*, 23−35. (b) Torchilin, V. P.; Lukyanov, A. N.; Gao, Z.; Papahadjopoulos-Sternberg, B. *Proc. Natl. Acad. Sci. U.S.A.* **2003**, *100*, 6039−6044.
(55) Torchilin, V. P.; Levchenko, T. S.; Rammohan, R.; Volodina, N.; Papahadjopoulos-Sternberg, B.; D'Souza, G. G. *Proc. Natl. Acad. Sci. U.S.A.* **2003**, *100*, 1972−1977.

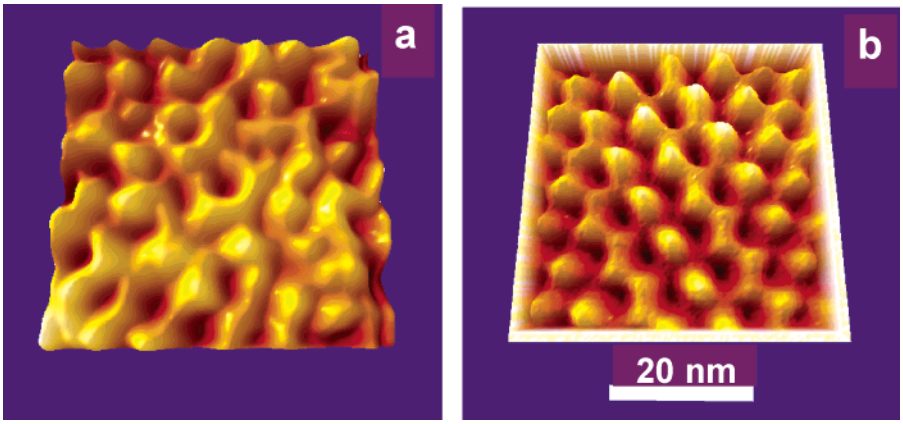

Figure 2. 3D reconstructions of freeze−fracture electron microscopy images of a chemically functionalized cubic lipid membrane MO/MTEG (MO is monoolein and MTEG is a double-chain synthetic lipid, 1-{8-[4-(*p*-maleimidophenyl)butaroylamino]-3,6-dioxaloctyl}-2,3-distearyl glyceryl DL-ether). The cubic structure was assembled at full hydration in excess aqueous buffer phase. (a) Raw image showing the presence of undulations in the complex fluid 3D cubic membrane. (b) Fourier-filtered image corresponding to the underlying matrix structure of the cubic liquid-crystalline freeze−fracture section.

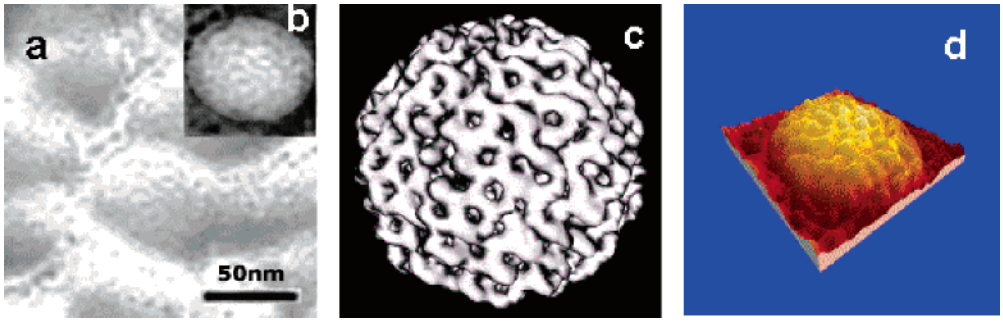

Figure 3. (a) FF-EM image of a nanocubosome in a proteocubosome sample (MO/MTEG/Fab immunoglobulin fragments/buffer) at full hydration. The inset (b) shows a selected area of the raw image (a), in which the image contrast was processed in order to remove the experimental shadows and to reveal the contour of the nano-object. (c) 3D modelization of a spherical nanocubosome involving random undulations of the nodal surfaces. The nano-object is generated using $N = 2058$ nodes to simulate the outer cubosome surface. It corresponds to an experimental nanocubosome with a radial section around 58 nm. (d) 3D reconstruction from image (b).

architectures of a double diamond type formed upon spontaneous lipid/protein assembly in excess of aqueous medium. The proteocubosome dissection along a fracture plane should elucidate the mechanism of protein nanoencapsulation and confinement in the triply periodic networks of fluid membranous interfaces and, eventually, the respective location of the biomacromolecules with regard to the aqueous nanopores. In proteocubosome systems, in contrast to single-crystal cubosomes,[23] it could be anticipated that the self-assembly cubic organization may locally deviate from a "perfect" 3D crystal structure owing to the distortions caused by the entrapped protein macromolecules.

The high-resolution FF-EM image in Figure 2a is compatible with an undulated cubic geometry that characterizes the internal structure of the functionalized 3D cubic membrane involving 2 mol % of the synthetic lipid MTEG. Figure 2b presents the corresponding filtered image, which exposes the underlying periodic structure after removal of the high-frequency fluctuations. The comparison of the images in panels a and b of Figure 2 indicates that the steric and hydration-induced modifications, introduced by the guest MTEG molecules, evidently cause changes in the local curvature of the lipid bilayer. This results in a pattern with lipid bilayer distortions (Figure 2a), which reflect the dynamic nature of the composite bicontinuous cubic membrane. In the presence of guest biomolecules, the cubic membrane architecture is no longer perfect as compared to the single-crystal systems of pure monoolein. Anisotropic patterns should be caused by local symmetry breaking.[56] It is remarkable that these distortions are generated on continuous interfaces rather than on single or punctual defects in the cubic lattice. The observed undulations of the 3D lipid membrane are typical for fluid-phase architectures. Such fluctuations imply that the aqueous nanochannels dynamically could open or close at cubosomic interfaces, thus affecting the exchange of molecules between the cubosome interior and the excess aqueous reservoir.

The internal proteocubosome nanostructure was investigated for the case of entrapment of water-soluble fragments (Fab) of the protein immunoglobulin in fully hydrated MO/MTEG cubic assemblies. In this case, the macromolecular size (extended length ~7 nm) is larger than the cubosomic aqueous nanochannel diameter ($D_w = 3.6$ nm). This steric incompatibility may induce local perturbations of the overall cubic supramolecular organization. Indeed, we found that the superstructure of the proteocubosome sample is generated from cubosomic nanodroplet substructures (nanocubosomes) of the kind presented in the FF-EM image in Figure 3a. The experimentally established nanocubosome shapes do not appear with protrusions of the lipid bilayer like those computed in Figure 1e,g. This confirms that the cubosome formation favors only selected N as stable 3D nanostructure configurations.

Regarding the location of the entrapped protein macromolecules in the supramolecular cubic structure, we suggest that

(56) Sadoc, J. F.; Mosseri, R. *Geometrical Frustration*; Cambridge University Press: Cambridge, UK, 1999.

they locate along the contact interfaces of the adjacent cubosomic nanodroplets (Figure 3a). The protein locations could be attributed to a defect network that tessellates the cubic lattice into an array of nanocubosomes. Comparison of Figures 2 and 3a indicates the local cubic topology modifications resulting in protein-induced nanocubosomic patterns. The image analysis reveals that the structural distortions caused by the guest lipid MTEG alone are not sufficiently significant to initiate the formation of a nanocubosome defect network in the generated patterns. In contrast, the incorporated large proteins do induce network defects in the periodic 3D supramolecular organization, which is the basis for the fragmentation of the bicontinuous cubic system into nanosized entities.

Figure 3d presents an example of a nanocubosome reconstructed in three dimensions. The nanocubosome is modeled in Figure 3c as a spherical cubosome, in which we introduced random undulations of the lipid membrane surface. This permitted us to account for the experimentally established fluctuations of the curved lipid bilayers constituting the cubosomic assembly. This approach represents the most realistic description yet available to model experimental cubosomic architectures. It yields nanocubosome shapes and sizes corroborating with the experimental results. In contrast, previous theoretical modelizations[52,53] refer principally to idealized solid structures based on single-crystal cubic models and perfect systems of aqueous channels. As a consequence, model cubosomes with interrupted channels with protrusions (which do not correspond to real situations) may come as output of the calculations for a given experimental cubosome size. The 3D fluctuations of the lipid bilayers constituting the cubosomic vehicles, which are experimentally established and theoretically modeled here, have not been previously taken into account.

This detailed study of the structure of a proteocubosome carrier, involving a protein that exceeds the size of the water nanochannels in the cubic lattice, revealed that the incorporated macromolecules induce 3D patterning of the overall cubic supramolecular architecture. Local frustrations by guest biomolecules do not necessarily imply that the lipid/protein cubic phase will be thermodynamically destabilized. General considerations on the influence of soluble proteins and hydration (limited or full hydration) conditions on the cubic mesophase stability and phase transformations were presented in ref 37. Incorporated proteins may modify the mean packing parameter of the amphiphilic mixture. As a consequence, the lipid monolayer curvature, the cubic lattice unit cell, and the associated aqueous nanochannel dimension and lipid bilayer thickness could be affected by the presence of the protein.

The location of a protein in the 3D self-assembled cubic architecture will depend on its hydrophobic−hydrophilic balance and its affinity for interaction with the lipid bilayer. Small proteins of amphiphilic nature are able to adsorb or penetrate into the lipid bilayer and, thus, to alter the mean interfacial curvature. Above a critical concentration, the guest protein could destabilize the host cubic lipid matrix and cause its transformation into new phases. Such effects were reported, for instance, with the protein cytochrome *c* embedded in monoolein cubic mesophases.[39,43] In contrast, the protein transferrin was found[38] to induce swelling of the monoolein cubic lattice without changing the space group symmetry.

Future studies should demonstrate the potential surface activity of therapeutic proteins of interest and their affinity to associate to lipid headgroup/water interfaces, as this could result in profound effects on the mean packing parameter and the cubic mesophase stability. Because the amino acid sequence and tertiary structural organization, determining eventual amphiphilic properties, are specific for every protein, it could not be speculated that the protein size is the principal factor that governs the accommodation of the macromolecule inside the aqueous nanochannels or at the interface boundaries of interconnected cubosomic nano-objects constituting the supramolecular assembly. In addition to the steric parameters, the interfacial activity of soluble proteins and their effect on the lipid hydration are important factors determining the partitioning of the protein macromolecules between the aqueous phase and the interfacial regions. When the proteins are smaller than about 16−20 kDa and they are of amphiphilic nature, it could not be guaranteed that they will partition preferentially inside the aqueous pores of the cubic supramolecular assembly, as they can show an affinity for the lipid bilayer.

Conclusion

The investigated proteocubosome complex fluid includes dynamic 3D membranous nanostructures. By comparison to single-crystal cubosome systems,[21a] we established that these supramolecular proteocubosomic nanostructures are built-up from fluctuating 3D bicontinuous cubic membranes enclosed in nano-object shapes. When the local fluctuations are large, the inherent open nanochannels may disrupt or close, which will reduce the cubosome capacity for release or uptake of soluble molecules. This effect could be used for controlling the release and uptake processes. Our results elucidate the mechanism by which a proteocubosomic object takes shape. Stable diamond-type cubosome formation is associated only with discrete sizes of the generated nanostructures. The smallest stable cubosomic entity requires 29 nodes in order to realize a diamond-type nanochannel system.

Acknowledgment. The comments of the reviewers are gratefully acknowledged.

JA060082C